2-Dimensional Human-Like Driver Model for Autonomous Vehicles in Mixed Traffic

M N Sharath [1], Nagendra R. Velaga [1*], Mohammed A. Quddus [2]

[1] Department of Civil Engineering, Indian Institute of Technology Bombay, Mumbai, India
[2] School of Civil and Building Engineering, Loughborough University, Loughborough, U.K
[*] n.r.velaga@iitb.ac.in

Abstract: Classical artificial potential approach of motion planning is extended for emulating human driving behaviour in two dimensions. Different stimulus parameters including type of ego-vehicle, type of obstacles, relative velocity, relative acceleration, and lane offset are used. All the surrounding vehicles are considered to influence drivers' decisions. No emphasis is laid on vehicle control; instead, an ego vehicle is assumed to reach the desired state. The study is on human-like driving behaviour modelling.

The developed motion planning algorithm formulates repulsive and attractive potentials in a data-driven way in contrast to the classical arbitrary formulation. Interaction between the stimulus parameters is explicitly considered by using multivariate cumulative distribution functions. Comparisons of two-dimensional (lateral and longitudinal) performance indicators with a baseline model and generative adversarial networks indicate the effectiveness and suitability of the developed motion planning algorithm in mixed traffic environment.

1. Introduction

The transition from human-driven to Autonomous Vehicles (AVs) may take several decades [1]. In the transition period, these two types of vehicles constitute *mixed traffic*. Coordination and cooperation between them are essential to ensure safety [2, 3]. AVs should also make the occupants and other road users feel safe [4]. AVs are publicly acceptable only if its driving behaviour is comprehensible and comparable to human drivers [5, 6]. Hence, the AVs need to emulate human-like driving behaviour.

Microscopic traffic parameters including speed, gap, and accelerations maintained by human drivers characterize their driving behaviour. A driving behaviour model is said to be human-like if it can replicate microscopic parameters that are equivalent to that of humans [7]. According to Waymo, human drivers drive by answering the following questions [8]:

(i) where am I?
(ii) what is around me?
(iii) what will happen next? and,
(iv) what should I do?

AVs should, therefore, be able to answer these questions to navigate through the mixed traffic. Vehicle localization module (or a map-matching algorithm) answers the first question for the AVs. Sensors used for environment perception respond to the next two questions. A *motion planning algorithm* addresses the fourth question. Its task is to determine the future position(s) (and other states including speed, heading, and acceleration) of an AV considering the states of the surrounding obstacles to safely and comfortably navigate through dynamic traffic [9]. Motion planning enables AVs to navigate through dynamic traffic. This study develops a human-like motion planning algorithm for AVs.

A review of recent literature presented in Table 1 indicates the inability of classical motion planning techniques to emulate human-like driving behaviour. Though the advanced machine learning and artificial intelligence techniques can learn to model human-like driving behaviour, they have issues regarding interpretability, require a large data set, and are computationally expensive [10]. Extending a classical model to perform human-like motion planning can alleviate these issues [11]. Artificial potential field approach is enhanced in this study to develop a human-like motion model.

Further, human drivers' responses are naturally derived from several stimuli, which are called stimulus parameters. Drivers' responses (in lateral and longitudinal directions) in this study are modelled as a function of seven stimulus parameters, as shown in Fig. 1:

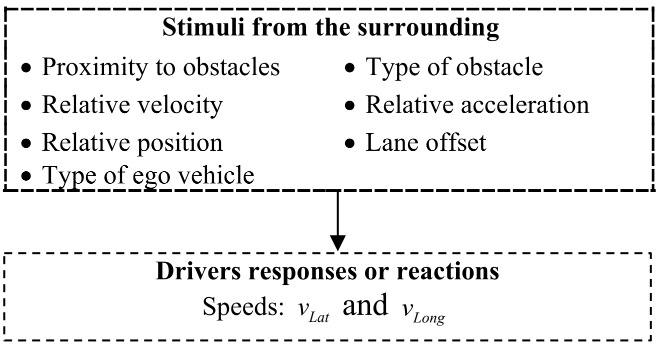

Fig. 1. *Stimuli-Response model used in the study*

where, v_{Lat} and v_{Long} respectively are lateral and longitudinal speeds.

The present study assumes that human drivers naturally try to minimize perceived threats. These threats are expressed as repulsive potentials around the obstacles. Reactions of drivers are generated based on these potentials. A reactive motion planning approach is adopted to address uncertain and dynamic environments [12].

Further, this study does not focus on vehicle control; instead, it assumes that an AV can attain the desired states, as suggested by the motion planner. The whole emphasis of this study is on emulating human-like driving behaviour in lateral and longitudinal directions to support AVs in mixed traffic. The subject vehicle is termed as Ego Vehicle (EV), which is an AV. Hence the terminologies AV and EV are interchangeably used.

2. Literature review

The motion planning algorithm developed in this study derives its inspiration from artificial potential field approach and hence termed as APF-MPA (Artificial Potential Fields-based Motion Planning Algorithm). A brief review of this approach is presented. The literature review also focuses on the factors enticing human drivers' reactions. Readers are referred to [9, 13–16] for recent literature on motion planning of autonomous land vehicles.

2.1. Artificial Potential Fields

The obstructions to an EV, be it static or dynamic, are termed as *obstacles* in this paper. Obstacles are to be avoided by the EV during navigation. In a nutshell, artificial potential field approach considers the obstacles to possess repulsive potentials to repel the EV. Repulsive forces are generated proportional to the repulsive potential field. These repulsive forces prevent the collision between an EV and the obstacles [17]. Similarly, a goal attracts the EV.

This empirical approach to motion planning is prevalent because of its ease in implementation and computational efficiency [18]. This approach is (i) collision-free, simple, and elegant, (ii) suitable for dynamic environment, and (iii) suitable for real-time applications [19]. It also permits to quantify the threat perceived by drivers. Threat from an obstacle is modelled as the repulsive potential around it. Artificial potential field approach allows the utilization of several stimulus parameters to develop a human-like driver model and thus is used in this study.

Human drivers perceive threats from surrounding obstacles and react. The parameters influencing human drivers' reactions are called *stimulus parameters.* They are:

1) Proximity between the EV and the obstacle, D
2) Angle between the EV's heading and the line joining EV and the obstacle, θ. This is referred to as *obstacle angle* in the rest of the paper.
3) Type of the EV, e
4) Type of the obstacle, o
5) Relative velocity between the EV and the obstacle along the line joining them, v_r
6) Relative acceleration between the EV and the obstacle along the line joining them, a_r
7) Lane offset of the EV, L, which is the distance measured from lane centre to the EV's centroid

Conventionally, the repulsive potential of an obstacle is modelled as the function of its proximity to the EV [17, 20]. Obstacles should strongly repel the EV when they are in close proximity to prevent a collision. A quadratic functional form of EV's proximity to the obstacle satisfies this criterion and is very popularly used [17, 21]. However, such an arbitrary formulation of the repulsive potentials may not reflect the way humans perceive the threat from the obstacles.

Further, studies considering vehicle type and relative acceleration are scarce [22]. For developing a human-like reactive motion planning model, it is necessary to define the functional form of repulsive potentials considering all the aforementioned stimulus parameters. A data-driven approach for the computation of repulsive/attractive potential and repulsive/attractive force is adopted in this study.

2.2. Factors Influencing Reaction of Human Drivers

Humans can perceive not only velocities but also the accelerations [23]. Acceleration of an EV and relative acceleration between the EV and the obstacles provide valuable information regarding the passengers' comfort and threat assessment. Similarly, the type of EV and type of obstacle play an essential role in EV's reaction [24, 25]. A review of recent literature reveals that some of the vital stimulus parameters such as the acceleration of the EV, accelerations of the obstacles, obstacle angle, and type of the obstacles are not comprehensively utilized in modelling the human driving behaviour. However, it is necessary to incorporate such valuable stimulus parameters to develop a robust human-like reactive motion model.

Further, existing artificial potential field approaches for motion planning consider the factors influencing drivers' behaviour to be independent. Different artificial potentials are defined for each factor. Superposition principle is then used to obtain the net potential. However, in reality, these factors may not be independent. For example, the separation maintained by a driver from an obstacle can be a function of relative velocity. Not just that, it can also depend upon the type of the ego vehicle, type of obstacle, and relative position of the obstacle. Interaction among these variables is difficult to model. So, the present study constructs multivariate cumulative distribution functions (CDFs) (a data-driven approach) and formulates the repulsive and attractive potential fields.

Additionally, drivers' reactions as per existing car-following models depend on stimuli from the leading vehicle [26–28]. However, drivers' reactions can be influenced by all the surrounding obstacles. Therefore, the reactions of the EV are assumed to be influenced by all the surrounding vehicles in this study. Existing lane-changing models can only determine the feasibility of a lane change, but do not describe the lane changing manoeuvre needed for lateral motion planning. Studies that model both lateral and longitudinal motion of a vehicle are scarce.

Moreover, most of the existing driving behaviour models ignore the influence of the type of obstacle in predicting drivers' reactions. This is primarily because of the near homogeneous traffic that prevails in most of the developed countries [29]. However, considering the type of vehicles in the model can result in a better human-like driver model. It is also a prerequisite for modelling heterogeneous traffic prevalent in developing economies.

Considering all the aforementioned drawbacks, a two-dimensional human-like driving behaviour model is developed in this study. Seven stimulus parameters are used. A data-driven approach is adopted for describing the artificial potentials, leaving no room for arbitrary assumptions.

Table 1 furnishes the different stimulus parameters (columns A to H) used in recent literature. Different fields used in Table 1 are described below it. Table 2 compares and contrasts the recent literature on motion planning, and also highlights the novelty of the present study.

Table 1 Stimulus parameters in recent human-like trajectory planning studies

Authors	A	B	C	D	E	F	G	H	I	J	K
[30] Sharath and Velaga (2020)	✓	✓			✓			✓	NGSIM	Enhanced intelligent driver model	SE
[31] Amini et al. (2018)	✓	✓			✓	✓			RD	Gazis-Herman-Rothery car-following model	n/a
[32] Greveling (2018)	✓				✓	✓	✓	✓	NGSIM	Wasserstein Generative Adversarial Imitation Learning	SE
[2] Li et al. (2018b)		✓			✓		✓		KI+SD	CNN + DMN	SE
[22] Lin et al. (2018)	✓	✓			✓				NGSIM	Multi-mode hybrid automaton model	n/a
[26] Wang et al. (2018)	✓	✓			✓				NGSIM	Gated Recurrent Unit	SE
[33] Zhang et al. (2018)	✓	✓			✓				NGSIM	Gaussian mixture model	SE
[34] Kuefler et al. (2017)	✓				✓	✓	✓	✓	NGSIM	Generative adversarial networks	SE
[35] Lee et al. (2017)	✓				✓				NGSIM	Discretionary lane change model	SE
[36] Zhou et al. (2017)	✓	✓			✓				NGSIM	Recurrent Neural Network	SE
[24] Ravishankar and Mathew (2011)	✓		✓	✓	✓	✓			NGSIM + RD	Modified Gipp's model	SE
Present study	✓	✓	✓	✓	✓	✓	✓	✓	NGSIM	Artificial potential method	SE

Name	Description	Name	Description	Name	Description
A	Velocity of EV	H	Obstacle angle	n/a	Not applicable
B	Velocity of obstacles	I	Data Used	NGSIM	Next Generation SIMulation
C	Acceleration of EV	J	Methodology	RD	Additional Real-world Data
D	Acceleration of obstacles	K	Testing environment	SD	Simulator Data
E	Headway	CNN	Convolutional Neural Network	SE	Simulation Environment
F	Type of EV and obstacles	DMN	Decision Making Network		
G	Lane offset	KI	KITTI vision dataset		

Table 2 Comparison of recent literature on motion planning

Type	Stimulus parameters	Lane keeping	Smooth Trajectory	Human-like	Suitability	Example studies
RRT	N	N	N	N	S	[37–39]
PRM	N	N	N	N	S	[40, 41]
Graph search	P*	N	N	N	S	[42, 43]
Visibility graph	N	N	N	N	D	[44]
Invariant Sets	P*	N	--	N	S	[45–47]
MPC	P*	Y	Y	N	D	[48, 49]
APF+ RN	P*	N	N	N	D	[50]
Deep learning	P**	N	Y	N	D	[51, 52]
GAN	P***	Y	Y	Y	D	[32, 34]
SVM	P*	N	Y	N	D	[53]
GMM	P*	Y	Y	N	D	[54]
IRL	P**	Y	Y	Y	D	[55, 56]
End-to-end learning	--	Y	Y	Y	D	[57]
Present study	Y	Y	Y	Y	D	

*	Only relative velocity and proximity are considered	**MPC**	Model Predictive Control
**	Relative speed, relative acceleration and proximity are considered	**N**	Not considered
***	Speed of subject vehicle, proximity, obstacle angle, lane offset and type of obstacle are considered	**P**	Partially considered
APF	Artificial Potential Field	**PRM**	Probabilistic Road Map
D	Dynamic Environment	**RN**	Resistance Network
GAN	Generative Adversarial Network	**RRT**	Rapidly exploring Random Trees
GMM	Gaussian Mixture Model	**S**	Static environment
IRL	Inverse Reinforcement Learning	**SVM**	Support Vector Machine
		Y	Yes

3. Proposed method

3.1. Significance of CDF

The probability that a random variable X taking a value less than or equal to x is defined by CDF($X \leq x$), where x is the realized value. In the context of motion planning, to highlight the significance of the CDF, a simple example is presented considering the proximity between an EV and obstacles as the random variable (proximity is the random variable X in this example). Empirical CDF(X) can be obtained by computing the proportion of observations that are less than x. Similarly, empirical multivariate CDF($X_1, X_2,..X_n$) can be obtained by computing the proportions of observations such that $X_1 \le x_1$, $X_2 \le x_2 \ldots X_n \le x_n$.

If the CDF of X is constructed (based on the realized values of proximities), the magnitude of the CDF at small values of x would be small. This indicates a few instances of proximities going below x. Whenever the proximity reduces, the driver of the EV reacts in a way to increase it to a preferred level. Small magnitudes of the CDF(X) (at a small value of x) can be the result of drivers' unwillingness to maintain small proximities (or short headways) with the obstacles. The same can be hypothesized as the willingness of drivers to *react* to increase the proximity. Therefore, 1-CDF(X) can be considered as the potency of drivers to react. It may also be interpreted as the potential of obstacles to repel the EV, which consequently elicits reactions from the drivers.

In the present empirical study, 1-CDF(X) is considered as the potential of obstacles to repel the EV. The human-driven trajectory data available in the NGSIM dataset is used to describe the repulsive potentials mentioned in Eq. (5) and (7) by finding empirical multivariate cumulative distributions. A similar concept of employing CDF for data-driven modelling is performed in [58].

3.2. Definitions and Overview

Potential of obstacles to repel the EV is supposed to depend on stimulus parameters. Accordingly, three different repulsive forces proportional to the repulsive potentials are assumed to arise as follows:

RF_1: Repulsive force resulting from the proximity between an EV and an obstacle. The lower the proximity, the higher the RF_1.

RF_2: Repulsive force arising from the relative velocity between an EV and an obstacle. The smaller the relative velocity, the greater the RF_2.

RF_3: Repulsive force as a result of the relative acceleration between an EV and the obstacle. The lesser the relative acceleration, the higher the RF_3. A negative value of relative velocity or relative acceleration suggests that the EV and the obstacle are moving towards each other.

Fig. 2 depicts the three components of the repulsive forces (RF_1, RF_2 and RF_3) exerted on an EV by surrounding obstacles (A, B and C). The centroids of the obstacles (EV is assumed to avail this information as a part of perception of environment) are taken as sources of artificial potentials and consequently generated repulsive forces. These repulsions prevent the collisions.

All the obstacles (e.g., vehicles) surrounding the EV are considered to influence its motion. Apart from the repulsive forces, the EV also experiences an attractive force proportional to its offset from the lane centre (which is not shown in Fig. 2). This attractive force enables the EV to track a lane and prevents it from going off the road. Larger the lane offset of the EV, larger is the attractive force (by definition, the magnitude of lane offset cannot exceed half the lane width). θ_A is the obstacle angle for obstacle A, where $0^0 \le \theta \le 180^0$. The magnitude of θ is around zero for obstacles ahead of the EV. Such obstacles invoke larger responses from drivers than obstacles behind the EV with larger θ.

The flowchart presented in Fig. 3 provides an overview of APF-MPA. At any given instant, seven stimulus parameters are used to compute the variables using Eq. (1) to (4) to perceive the environment. The information generated during the calibration phase is then utilized to estimate the total repulsive and attractive forces acting on the EV using Eq. (9) to (11). The repulsive and attractive forces are eventually translated into the required displacement of the vehicle in Eq. (14) and (15). This information is then passed on to the vehicle control module for necessary actions. These steps are repeatedly performed at every time epoch.

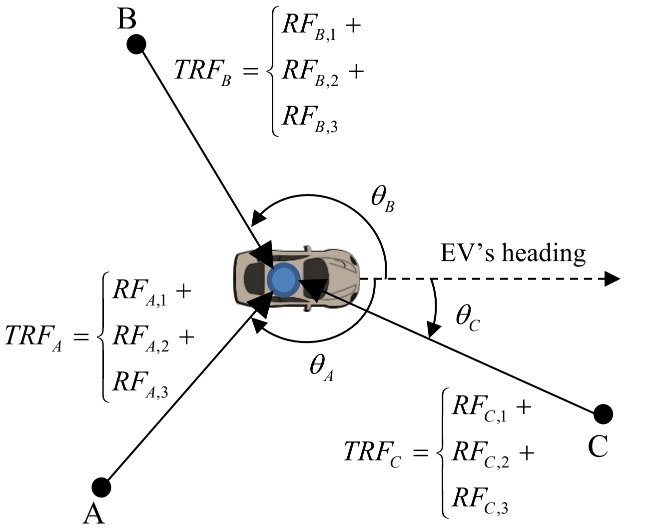

Fig. 2. *Repulsive forces of different obstacles*

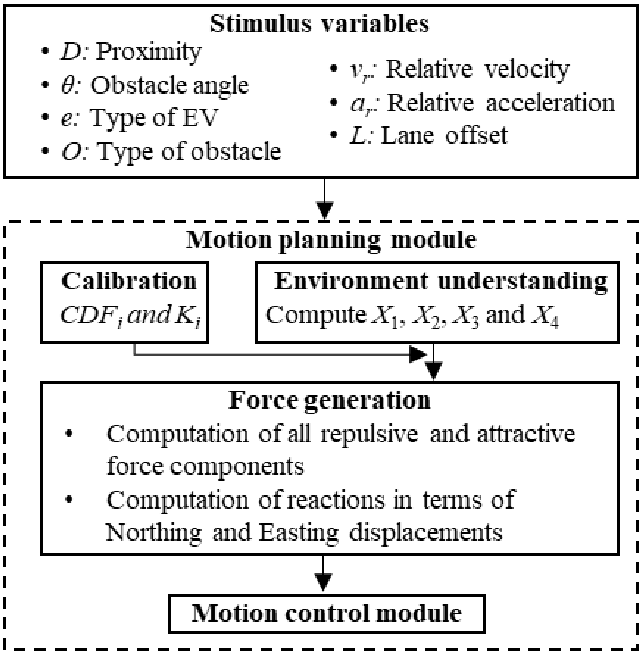

Fig. 3. *Flowchart of the proposed trajectory planning algorithm*

3.3. Environment Understanding

Seven stimulus parameters (see Section 2.1) are considered to influence the reactions of human drivers. Hence, they are used to formulate four reaction inducing variables. For a given EV-Obstacle pair (e.g., car-truck), and at any given time instant, reaction inducing variables are defined as follows:

$$X_1 = \{D,\ \theta, v_r\} \tag{1}$$

$$X_2 = v_r \times |v_{EV}| \tag{2}$$

$$X_3 = a_r \times |a_{EV}| \tag{3}$$

$$X_4 = L_{EV} \tag{4}$$

where,

D is proximity between an EV and an obstacle (m);

θ is obstacle angle (degrees);

v_r is relative velocity between the EV and the obstacle along the line joining them (ms^{-1});

a_r is the relative acceleration between the EV and the obstacle along the line joining them (ms^{-2});

$|v_{EV}|$ is magnitude of velocity of the EV (ms^{-1});

$|a_{EV}|$ is magnitude of acceleration of the EV (ms^{-2});

L_{EV} is lane offset of the EV (m);

3.4. Description of Reaction Inducing Variables

X_1 : Proximity between an EV and an obstacle is popularly considered to describe the repulsive potential in the literature [22, 26]. However, the interactions among the stimulus variables are ignored. In this study, X_1 is a variable that explicitly considers the interactions between the five variables: proximity, obstacle angle, relative speed, type of ego vehicle, and type of obstacle.

X_2 and X_3 : Formulations of the repulsive potentials based on relative velocity and relative acceleration are done in the past [26, 31]. However, these formulations have a disadvantage; a large magnitude of negative relative velocity or negative relative acceleration may be possible due to the motion of the obstacles despite the EV being at rest, warranting reactions from EV, which is preposterous. Whereas, a large magnitude of negative relative velocity or acceleration when the EV is moving at high velocity or acceleration should demand a response from the EV. This issue can be adequately addressed by considering the instantaneous velocity and instantaneous acceleration of the EV as shown in Eq. (2) and (3). The approach renders the repulsive potentials arising due to relative velocity and relative acceleration adaptive. X_2 explicitly considers the interaction between relative velocity, type of obstacle and type of EV while X_3 between relative acceleration, type of obstacle and type of EV.

X_4 : Lane offset of an EV indicates its lateral position. An attractive force is generated proportional to the lane offset to motivate the EV to travel along the centreline of a lane. Attractive potential thus arising is described considering the interaction between lane offset, type of EV, and type of obstacle.

3.5. Generation of Attractive and Repulsive Forces

Traditionally, the negative gradient of an arbitrarily defined potential field is considered as the force. A data-driven approach is adopted in this study to describe artificial potentials. The three repulsive potentials and corresponding repulsive forces are described as shown in Eq. (5) and (6). The attractive potential and the corresponding attractive force are provided as in Eq. (7) and (8).

$$RP_j = 1 - CDF(X_j) \qquad \forall j = 1 \text{ to } 3 \tag{5}$$

$$RF_j = K_j \times RP_j \qquad \forall j = 1 \text{ to } 3 \tag{6}$$

$$AP = CDF(X_4) \tag{7}$$

$$AF = K_4 \times AP \tag{8}$$

where, RP_j is the j^{th} constituent of the repulsive potential; $CDF(X_j)$ is the value of cumulative distribution function of the variable X_j ; RF_j is the j^{th} constituent of repulsive force. All these force constituents are oriented along the line joining an obstacle and an EV; AP is the attractive potential developed due to the lateral offset of an EV; AF is the attractive force with which the lane centre attracts an EV; and K_j is the j^{th} conversion factor that converts the repulsive/attractive potential to repulsive/attractive force.

Total repulsive force from an obstacle to EV is obtained as:

$$TRF = \sum_{j=1}^{3} RF_j \qquad \forall \text{ obstacles} \tag{9}$$

Lateral and longitudinal components of this total repulsive force is obtained as:

$$TRF_{Lat} = \cos(\theta) \times TRF \qquad \forall \text{ obstacles} \tag{10}$$

$$TRF_{Long} = \sin(\theta) \times TRF \qquad \forall \text{ obstacles} \tag{11}$$

Attractive force due to lane offset has only a lateral component. The net force on the EV due to repulsive and attractive forces from all the surrounding obstacles is resolved into lateral and longitudinal components as:

$$NF_{Lat} = \left(\sum_{\forall \text{ obstacles}} TRF_{Lat} \right) + AF \tag{12}$$

$$NF_{Long} = \sum_{\forall \text{ obstacles}} TRF_{Long} + \mathrm{N}(0,\ 0.02) \tag{13}$$

A small Gaussian perturbation like in [57] is added in Eq. (13) to avoid getting stuck in local minima. The net force incites reactions in the EV. In the present study, the reactions are expressed in terms of velocity of the EV as done in [59]. Therefore, NF_{Lat} and NF_{Long} are used as terms to correct the desired speeds respectively in lateral and longitudinal directions. The position update equations are:

$$\hat{P}_{Lat}^{t+\Delta t} = \hat{P}_{Lat}^{t} + \left(DesiredSpeed_{Lat} + NF_{Lat}^{t} \right) \times \Delta t \tag{14}$$

$$\hat{P}_{Long}^{t+\Delta t} = \hat{P}_{Long}^{t} + \left(DesiredSpeed_{Long} + NF_{Long}^{t} \right) \times \Delta t \tag{15}$$

where, $\hat{P}_{Lat}^{t}$ and $\hat{P}_{Long}^{t}$ are the estimated lateral and longitudinal components of the position of an EV at time *t*. $\hat{P}_{Lat}^{t+\Delta t}$ and $\hat{P}_{Long}^{t+\Delta t}$ are the estimated lateral and longitudinal components of the position to be occupied by the EV in the subsequent time epoch. Δt is the time step, considered to be 0.1s.

Desired speed in lateral direction is taken as 0, while that in longitudinal direction is a parameter to be calibrated. Eq. (14) and (15) provide the future position of the EV by applying a correction to the desired lateral and longitudinal positions. The equations are dimensionally homogeneous as K_j have dimensions of speed.

4. Performance evaluation

4.1. Data Used

Next Generation SIMulation (NGSIM) data of the US-101 highway collected from 7:50 AM to 8:35 AM, on 15 June 2005 is used in the study [60]. The data has trajectories of 6,101 human-driven vehicles, each of which is approximately 630m long (about 60 seconds, sampled at 10Hz). The freeway has five lanes and an auxiliary lane connecting a ramp. Any vehicle that enters the ramp is ignored, leaving us with trajectories of 5,470 vehicles as provided in Table 3.

Table 3 Classification of NGSIM dataset used

SL No.	Class	Calibration	Validation
1	Bike	26	12
2	Car	3714	1591
3	Truck	89	38

Ignoring the vehicles does not mean the corresponding trajectories are deleted from the database, but the responses of the ignored vehicles are not modelled. However, the stimuli caused by such vehicles on the remaining trajectories are considered. Trajectory data is smoothed to reduce noise according to [61]. A more sophisticated trajectory reconstruction technique developed by [62, 63] may also be used to reduce errors in the trajectories. The NGSIM dataset has three categories of vehicles: bike, car, and truck. Table 3 provides the number of trajectories available in each category. 70% of the trajectories are randomly used for calibration and the remaining 30% for validation. The dataset encompasses trajectories exhibiting lane-changing and vehicle following behaviours.

4.2. Calibration

Reaction inducing variables are assumed to govern the reactions of drivers. Their distribution, extracted from the actual human-driven trajectory data, can prove essential in the development of a human-like driver model. Reaction inducing variables are computed for every epoch and for all the trajectories using Eq. (1) to (4). As their distributions do not follow any standard distribution, empirical multivariate CDFs are constructed from human-driven trajectory data.

Fig. 4 depicts the repulsive potential due to relative velocity and relative acceleration, whereas Fig. 5 exhibits attractive potential due to lane offset. Fig. 6 portrays the repulsive potential due to X_1 for a particular case of Car-Car (EV-Obstacle) interaction. The darker the colour, the higher is the repulsive potential.

A sharp gradient can be noticed in Fig. 6 whenever $v_r < 0$. This suggests that the drivers efficiently perceive the relative velocity and react as the v_r tends negative. Further, referring to Fig. 6, the repulsive potential is high for smaller proximities. Obstacles in front of EV (the obstacle angle θ would be around 0^0) incite greater responses than obstacles that are behind (with larger θ values). This can be observed in Fig. 6, where the white region (with lesser repulsive potential) increases with an increase in θ.

The differences between these distributions can be observed in Fig. 4, Fig. 5, and Fig. 6. This serves as clear evidence that highlights the importance of considering multiple stimulus parameters in motion planning. This finding also aligns with [24, 29, 31, 64].

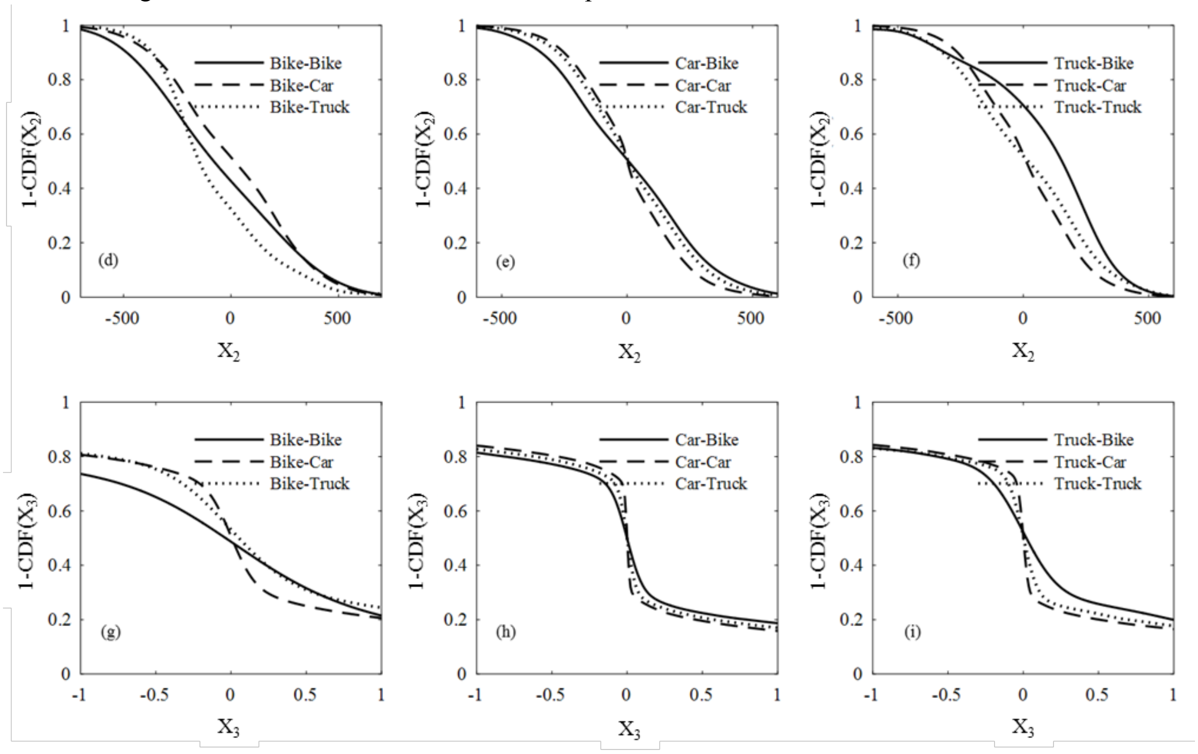

Fig. 4. *Repulsive potential due to X_2 and X_3 for different EV-Obstacle pairs*

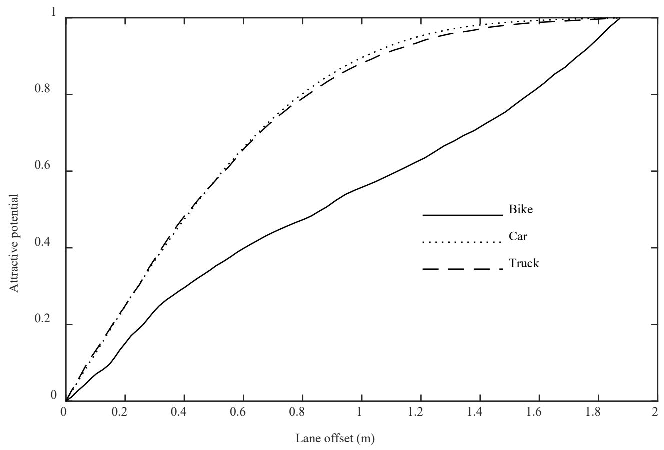

Fig. 5. *Attractive potential due to X_4*

The magnitude of K_j which converts attractive/ repulsive potential to the attractive/repulsive force has an effect on reactions of the EV as described by Eq. (6) and (8). Identifying the optimal combination of K_j for different EV-Obstacle combinations is key to the performance of the human-like driver model. For this reason, radial error, a performance measure is defined as shown in Eq. (16), similar to the definition in [26]. Since the radial error is a function of simulation horizon, the trajectory length is restricted to 10s as done in [34]. Radial error is given by:

$$RE = \sqrt{\frac{1}{T}\sum_{i=1}^{T}\left(\frac{1}{100}\sum_{t=1}^{100}\left[\left(P^{t}_{Lat,i}-\hat{P}^{t}_{Lat,i}\right)^{2}+\left(P^{t}_{Long,i}-\hat{P}^{t}_{Long,i}\right)^{2}\right]\right)} \quad (16)$$

where, T is total number of trajectories; $P^{t}_{Lat,i}$ and $P^{t}_{Long,i}$ are the observed lateral and longitudinal positions of the EV at time t.

K_1, K_2 and K_3 are considered in the range between 5 and 10m/s with a step-size of 1m/s. K_4 is considered between 0 and 1m/s with a step-size of 0.2m/s. $DesiredSpeed_{Long}$ is taken in the range from 12 to 18m/s with a step-size of 1m/s. For all possible combinations of these parameters (systematic brute-force approach), the resulting radial errors using calibration trajectories are logged. The combination leading to the least magnitude of radial error is considered as the optimal combination. Mean and standard deviation of parameters calibrated at driver level are provided in Table 4.

Table 4 Calibration result

EV Type	Bike	Car	Truck
K_1 (m/s)	6.62 (1.46)	7.42 (3.34)	7.86 (3.40)
K_2 (m/s)	7.60 (2.46)	6.02 (2.28)	6.34 (2.27)
K_3 (m/s)	6.35 (2.30)	8.47 (3.73)	6.60 (3.42)
K_4 (m/s)	0.25 (0.10)	0.72 (0.33)	0.62 (0.37)
$DesiredSpeed_{Long}$ (m/s)	14.5 (3.02)	13.1 (1.21)	12.4 (0.52)
Radial error (m)	5.53 (4.10)	3.83 (2.98)	4.03 (4.29)

4.3. Baseline Model

The popular intelligent driver model (IDM) is integrated with MOBIL lane-change model and is used as a baseline model to compare the performance [65, 66]. The parameters of IDM+MOBIL model are borrowed from [34], which also used the NGSIM dataset. Kuefler et al. have developed several generative adversarial networks for two-dimensional human driver modelling [34]. This study also compares those machine learning approaches with the APF-MPA.

4.4. Validation

The calibrated parameters are considered to be normally distributed with mean and standard deviation, as shown in Table 4. For each validation trajectory, the parameters are randomly chosen from Table 4. Instead of creating a hypothetical scenario for the simulation, the rich human-driving data available in the NGSIM dataset is used. A vehicle is randomly chosen and considered as an EV. The movements of all other vehicles are considered to happen according to the NGSIM dataset. The initial state of the EV is obtained from the NGSIM dataset. The variables that govern reactions of EV are determined using Eq. (1) to (4).

Reactions of the EV are then computed dynamically for subsequent epochs as per the Eq. (5) to (13). The motion of the EV during the subsequent time epochs is then modelled by Eq. (14) and (15). The process is repeated for all the validation vehicles, one at a time.

For a simulated variable v, the root weighted squared error is computed for all validation trajectories and for all time epochs as:

$$RWSE = \sqrt{\frac{1}{m}\sum_{i=1}^{m}\left(v^{i,t}_{sim}-v^{i,t}_{obs}\right)^{2}} \quad (17)$$

where m is the number of validation trajectories, v can be position or speed or lane offset. Subscripts *sim* and *obs* respectively indicate the simulated and observed values.

Fig. 7 provides the evolution of root weighted squared error for different variables. APF-MPA consistently outperforms the baseline IDM+MOBIL model. Compared to results reported in Keulfer et al. [34], root weighted squared error of different variables after 10s is better (or at par with) than several generative adversarial networks. The advantage of using attractive force to motivate the EV to keep lane is evident where the lane offset is about 0.5m.

Further, Fig. 8 to Fig. 11 exhibit the two-dimensional performance of APF-MPA. Fig. 8 and Fig. 9 respectively portray the distributions of acceleration and speed in longitudinal direction. A larger number of 0 accelerations is generated, thereby reducing the oscillations shown by human drivers about 0 accelerations. The longitudinal speed distribution appears to be similar to that of the observed distribution.

Fig. 10 and Fig. 11 respectively furnish the distribution of acceleration and speed in lateral direction. APF-MPA models larger magnitude of negative or positive accelerations similar to that of the observed accelerations. The distribution of lateral speed is also similar to the observed distribution.

The attractive force prevents the EV from going off the road while the repulsive forces from the surrounding vehicles prevent the collision. The occasional collisions experienced by the EV could be due to the hard-coded motion of the surrounding vehicles without regarding the presence of the EV. If the surrounding vehicles are imparted the capability to react to the presence of EV, we believe that all the collisions can be avoided.

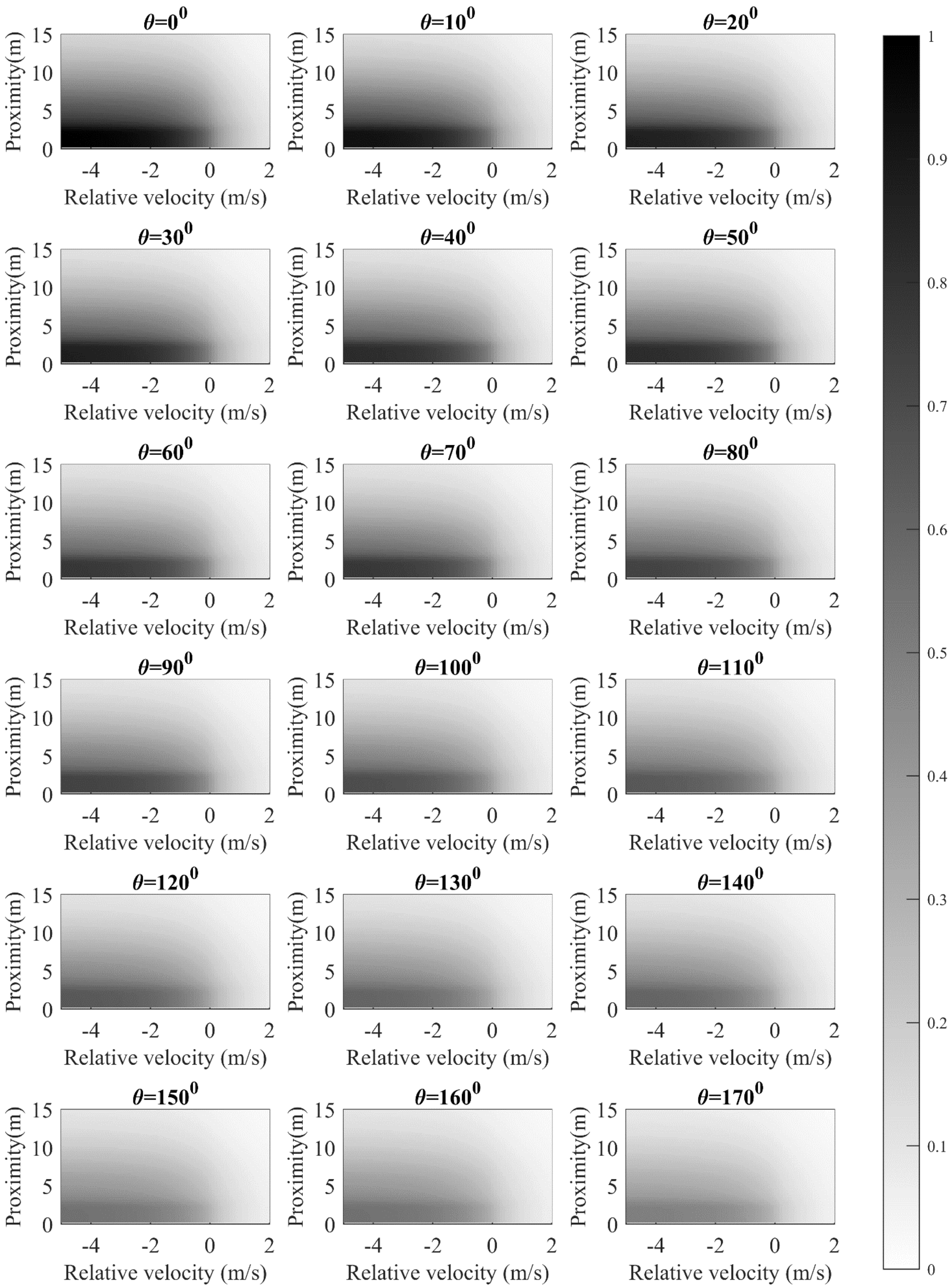

Fig. 6. *Repulsive potential due to X_1 for Car-Car (EV-Obstacle) interaction. Darker the colour, greater is the reactive potential*

The lateral and longitudinal performance measures presented in Fig. 7 to Fig. 11 indicate that APF-MPA can simultaneously model human-like vehicle-following and lane-changing behaviour. It can perform at par or better than generative adversarial networks presented in [34].

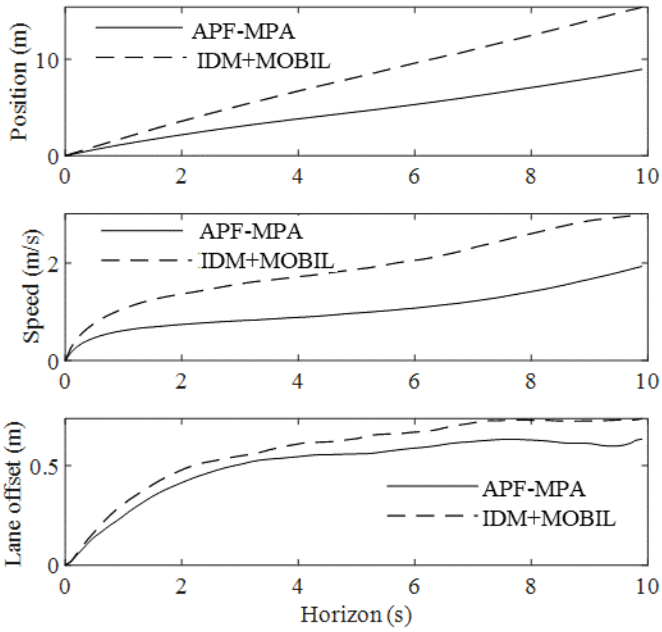

Fig. 7. Evolution of RWSE over a horizon of 10s

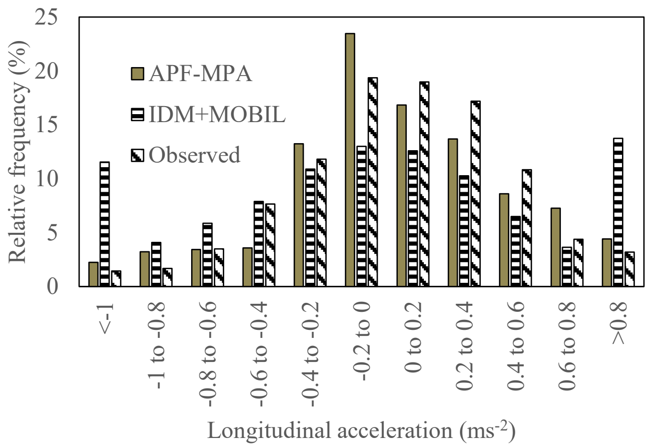

Fig. 8. Distribution of Longitudinal acceleration

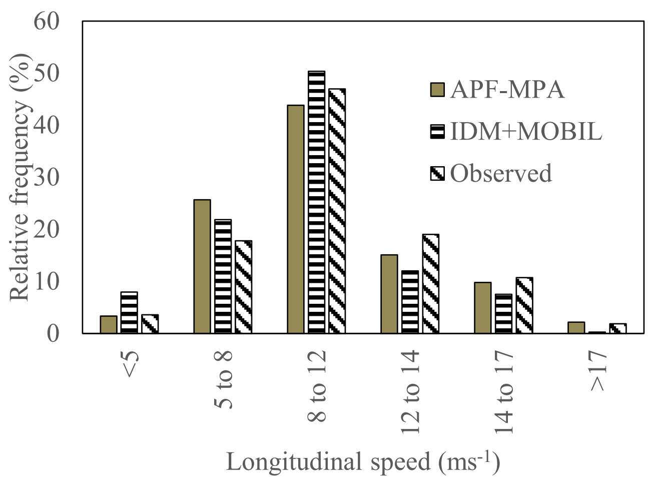

Fig. 9. Distribution of longitudinal speed

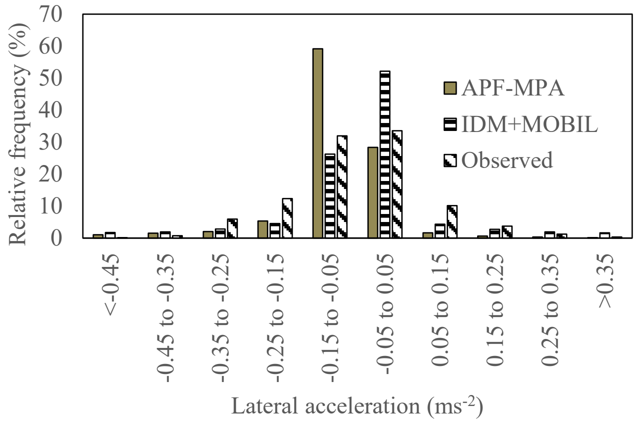

Fig. 10. Distribution of lateral acceleration

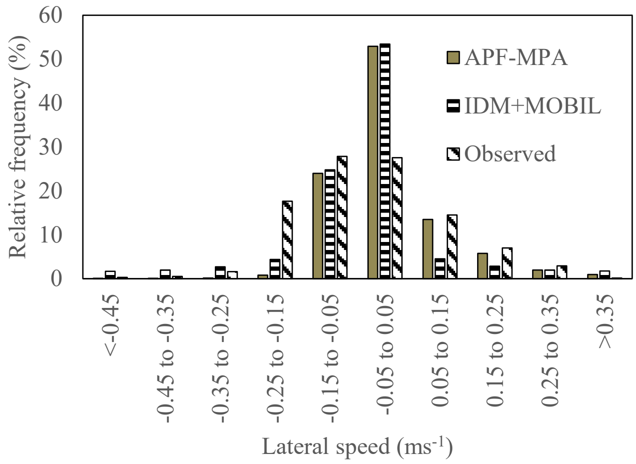

Fig. 11. Distribution of lateral speed

The distributions provided in Fig. 7 to Fig. 11 are compared with the observed distributions using Kullback-Leibler (K-L) divergence test and the divergence values are reported in Table 5. Smaller the divergence value, the higher is the conformity between the two distributions being compared.

Table 5 K-L divergence values

Performance measure	APF-MPA	IDM+MOBIL
Longitudinal acceleration	0.020	0.090
Lateral acceleration	0.127	0.070
Longitudinal speed	0.010	0.020
Lateral speed	0.220	0.137

Calibration and validation are performed for different types of vehicles. However, the measures provided in Fig. 7 to Fig. 11 and Table 5 indicate the combined performance of cars, bikes, and trucks. Validation results for bikes and trucks are not separately furnished due to the limited number of trajectories. Furthermore, the algorithm can process data at over 300Hz on Intel i7 3.4GHz processor with 8GB RAM, rendering it suitable for real-time applications.

The NGSIM dataset has known inaccuracies. Therefore, it is advisable to calibrate and validate APF-MPA with recently collected precise trajectory datasets like highD [67]. The methodology provided in this paper may be employed to model driving behaviour in different operating domains (such as intersections and curves).

5. Conclusions

The classical artificial approach of motion planning is extended to obtain human-like driving behaviour of autonomous vehicles in a mixed environment. Several stimulus information including the type of an ego vehicle, type of obstacles, proximity, obstacle angle, lane offset, velocities, and accelerations of the ego vehicle as well as those of obstacles are considered to emulate the human drivers' behaviour.

Multivariate cumulative distribution functions of the reaction inducing variables are computed to define attractive and repulsive potentials. The explicit consideration of multivariate interactions and the influence of all the surrounding vehicles on drivers' reactions resulted in the development of a human-like driver model, which can address both car following and lane changing behaviour. The novelty and contributions of this study are presented below:

1. **Extension of classical potential field method**: This study enhances the artificial potential field method to develop a human-like motion model to overcome the drawbacks of machine learning approaches.
2. **Data-driven approach**: Existing artificial potential field approaches describe the shape of the potential function arbitrarily [68, 69]. However, a data-driven approach is incorporated in this study to describe the potential fields. This approach can address complex driving behaviours, which cannot be modelled by arbitrary formulations.
3. **Stimulus parameters and their interactions**: Several stimulus parameters were used to develop a human-like motion model. Multiple stimulus parameters were simultaneously used in describing artificial potential fields. Instead of resorting to the conventional superposition approach, multivariate cumulative distribution functions are applied in this study.
4. **Application of multivariate CDF**: Artificial potential fields are described in a data-driven way by using multivariate CDFs. This approach also permitted the incorporation of interactions which may exist between stimulus parameters.
5. **Two-dimensional motion model**: Existing studies primarily concentrate either on vehicle-following or lane-changing behaviour (e.g., [70]). Any non-trivial vehicle motion will have both lateral and longitudinal components and are inseparable. The interaction between the lateral and longitudinal motions is ignored if they are studied separately [51]. Therefore, this study develops a two dimensional (lateral and longitudinal), human-like motion model.

Like humans, APF-MPA considers several stimulus parameters for human-like motion planning. However, obtaining some of these stimulus parameters like type or acceleration of an obstacle, in real-time, may not be easy. The hardware requirements for such a task can be economically prohibitive. This issue may be alleviated with V2V communication. Computer vision techniques may also be used for this purpose [71].

The difference in obstacles has been accounted while generating human-like responses in this study. There is a scope to support the society of automotive engineers level 2 or 3 [72] autonomous vehicles in a heterogeneous and mixed traffic environment. The research on AVs in developing countries may consequentially be accelerated. Further, APF-MPA may be used in a microscopic traffic simulation model. It may be possible to account stimuli from multiple vehicles and comprehensively model complex interactions between different types of vehicles in the simulation. Consequently, the safety and traffic performance parameters of mixed traffic may be adequately studied. The human-like driving behaviour of APF-MPA promotes social acceptance and may subsequently accelerate the adoption of autonomous vehicles.

Lastly, it would be interesting to study the changes in the traffic parameters due to the increase in the proportion of autonomous vehicles. Incorporation of the stimulus information in the machine learning models has a great potential to analyze the human-driving behaviour aptly. Using microscopic simulations, this study may be extended to understand safety and performance implications of autonomous vehicles in the mixed traffic environment.

6. References

[1] Litman, T.: 'Autonomous Vehicle Implementation Predictions Implications', (Victoria Transport Policy Institute, 2020)

[2] Li, L., Ota, K., Dong, M.: 'Humanlike Driving: Empirical Decision-Making System for Autonomous Vehicles', IEEE Trans. Veh. Technol., 2018, 67, (8), pp. 6814–6823

[3] Song, W., Xiong, G., Chen, H.: 'Intention-Aware Autonomous Driving Decision-Making in an Uncontrolled Intersection', Math. Probl. Eng., 2016, pp. 1–15

[4] Guo, C., Kidono, K., Terashima, R., et al.: 'Toward Human-like Behavior Generation in Urban Environment Based on Markov Decision Process With Hybrid Potential Maps', 2018 IEEE Intell. Veh. Symp. 2018, Suzhou, China, pp. 2209–2215

[5] Guo, C., Kidono, K., Machida, T., et al.: 'Human-like behavior generation for intelligent vehicles in urban environment based on a hybrid potential map', 2017 IEEE Intell. Veh. Symp. 2017, pp. 197–203

[6] Naumann, M., Lauer, M., Stiller, C.: 'Generating Comfortable, Safe and Comprehensible Trajectories for Automated Vehicles in Mixed Traffic', 2018 21st Int. Conf. Intell. Transp. Syst. 2018, pp. 575–582

[7] Zhu, M., Wang, X., Wang, Y.: 'Human-like autonomous car-following model with deep reinforcement learning', Transp. Res. Part C Emerg. Technol., 2018, 97, (October), pp. 348–368

[8] Waymo., L.L.C.: 'Waymo Safety Report: On the Road to Fully Self-Driving', (2018)

[9] Katrakazas, C., Quddus, M.A., Chen, W.-H., et al.: 'Real-time motion planning methods for autonomous on-road driving: State-of-the-art and future research directions', Transp. Res. Part C Emerg. Technol., 2015, 60, pp. 416–442

[10] Reichstein, M., Camps-Valls, G., Stevens, B., et al.: 'Deep learning and process understanding for data-driven Earth system science', Nature, 2019, 566, (7743), pp. 195–204

[11] Bazghandi, A.: 'Techniques, Advantages and Problems of Agent Based Modeling for Traffic Simulation', Int. J. Comput. Sci. Issues, 2012, 9, (1), pp. 115–119

[12] Subosits, J.K., Gerdes, J.C.: ‘From the Racetrack to the Road: Real-Time Trajectory Replanning for Autonomous Driving’, IEEE Trans. Intell. Veh., 2019, 4, (2), pp. 309–320
[13] Kala, R.: ‘On-Road Intelligent Vehicles’, (Elsevier, 2016, First)
[14] Gonzalez, D., Perez, J., Milanes, V., et al.: ‘A Review of Motion Planning Techniques for Automated Vehicles’, IEEE Trans. Intell. Transp. Syst., 2016, 17, (4), pp. 1135–1145
[15] Paden, B., Cap, M., Yong, S.Z., et al.: ‘A Survey of Motion Planning and Control Techniques for Self-Driving Urban Vehicles’, IEEE Trans. Intell. Veh., 2016, 1, (1), pp. 33–55
[16] Guanetti, J., Kim, Y., Borrelli, F.: ‘Control of connected and automated vehicles: State of the art and future challenges’, Annu. Rev. Control, 2018, (March), pp. 0–1
[17] Khatib, O.: ‘Real-time obstacle avoidance for manipulators and mobile robots’, Proceedings. 1985 IEEE Int. Conf. Robot. Autom. 1985, pp. 500–505
[18] Latombe, J.-C.: ‘Potential Field Methods’, (Ed.): ‘Robot Motion Planning’, (Springer US, 1991), pp. 295–355
[19] Sabudin, E., Omar, R., Che Ku Melor, C.: ‘Potential field methods and their inherent approaches for path planning’, ARPN J. Eng. Appl. Sci., 2016, 11, (18), pp. 10801–10805
[20] Ren, Y., Zheng, L., Khajepour, A.: ‘Integrated model predictive and torque vectoring control for path tracking of 4-wheel-driven autonomous vehicles’, IET Intell. Transp. Syst., 2019, 13, (1), pp. 98–107
[21] Hongbo, W., Li, C., Weihua, Z.: ‘Lane-keeping control based on an improved artificial potential method and coordination of steering/braking systems’, IET Intell. Transp. Syst., 2019, 13, (12), pp. 1832–1842
[22] Lin, Q., Zhang, Y., Verwer, S., et al.: ‘MOHA: A Multi-Mode Hybrid Automaton Model for Learning Car-Following Behaviors’, IEEE Trans. Intell. Transp. Syst., 2019, 20, (2), pp. 790–796
[23] Todd, J.T.: ‘Visual information about moving objects.’, J. Exp. Psychol. Hum. Percept. Perform., 1981, 7, (4), pp. 795–810
[24] Ravishankar, K.V.R., Mathew, T. V.: ‘Vehicle-Type Dependent Car-Following Model for Heterogeneous Traffic Conditions’, J. Transp. Eng., 2011, 137, (11), pp. 775–781
[25] Asaithambi, G., Kanagaraj, V., Srinivasan, K.K., et al.: ‘Study of traffic flow characteristics using different vehicle-following models under mixed traffic conditions’, Transp. Lett., 2018, 10, (2), pp. 92–103
[26] Wang, X., Jiang, R., Li, L., et al.: ‘Capturing Car-Following Behaviors by Deep Learning’, IEEE Trans. Intell. Transp. Syst., 2018, 19, (3), pp. 910–920
[27] Hao, S., Yang, L., Shi, Y.: ‘Data-driven car-following model based on rough set theory’, IET Intell. Transp. Syst., 2018, 12, (1), pp. 49–57
[28] Cattin, J., Leclercq, L., Pereyron, F., et al.: ‘Calibration of Gipps’ car-following model for trucks and the impacts on fuel consumption estimation’, IET Intell. Transp. Syst., 2019, 13, (2), pp. 367–375
[29] Ye, F., Zhang, Y.: ‘Vehicle Type–Specific Headway Analysis Using Freeway Traffic Data’, Transp. Res. Rec. J. Transp. Res. Board, 2009, 2124, (1), pp. 222–230
[30] Sharath, M.N., Velaga, N.R.: ‘Enhanced intelligent driver model for two-dimensional motion planning in mixed traffic’, Transp. Res. Part C Emerg. Technol., 2020, 120, (September), p. 102780
[31] Amini, E., Tabibi, M., Khansari, E.R., et al.: ‘A vehicle type-based approach to model car following behaviors in simulation programs (case study: Car-motorcycle following behavior)’, IATSS Res., 2019, 43, (1), pp. 14–20
[32] Greveling, D.P.: ‘Modelling human driving behaviour using Generative Adversarial Networks’, University of Groningen, 2018
[33] Zhang, Y., Lin, Q., Wang, J., et al.: ‘Lane-Change Intention Estimation for Car-Following Control in Autonomous Driving’, IEEE Trans. Intell. Veh., 2018, 3, (3), pp. 276–286
[34] Kuefler, A., Morton, J., Wheeler, T., et al.: ‘Imitating driver behavior with generative adversarial networks’, 2017 IEEE Intell. Veh. Symp. 2017, Redondo Beach, CA, pp. 204–211
[35] Lee, J., Park, M., Yeo, H.: ‘A probability model for discretionary lane changes in highways’, KSCE J. Civ. Eng., 2016, 20, (7), pp. 2938–2946
[36] Zhou, M., Qu, X., Li, X.: ‘A recurrent neural network based microscopic car following model to predict traffic oscillation’, Transp. Res. Part C Emerg. Technol., 2017, 84, pp. 245–264
[37] Qureshi, A.H., Ayaz, Y.: ‘Intelligent bidirectional rapidly-exploring random trees for optimal motion planning in complex cluttered environments’, Rob. Auton. Syst., 2015, 68, pp. 1–11
[38] Moon, C., Chung, W.: ‘Practical probabilistic trajectory planning scheme based on the Rapidly-Exploring Random Trees for two-wheeled mobile robots’, Int. J. Precis. Eng. Manuf., 2016, 17, (5), pp. 591–596
[39] Arslan, O., Berntorp, K., Tsiotras, P.: ‘Sampling-based algorithms for optimal motion planning using closed-loop prediction’, 2017 IEEE Int. Conf. Robot. Autom. 2017, pp. 4991–4996
[40] Mohanta, J.C., Keshari, A.: ‘A knowledge based fuzzy-probabilistic roadmap method for mobile robot navigation’, Appl. Soft Comput., 2019, 79, pp. 391–409
[41] Berntorp, K., Hoang, T., Di Cairano, S.: ‘Motion Planning of Autonomous Road Vehicles by Particle Filtering’, IEEE Trans. Intell. Veh., 2019, 4, (2), pp. 197–210
[42] Gu, T., Dolan, J.M., Lee, J.-W.: ‘Human-like planning of swerve maneuvers for autonomous vehicles’, 2016 IEEE Intell. Veh. Symp. 2016, pp. 716–721
[43] Karaman, S., Frazzoli, E.: ‘Sampling-based algorithms for optimal motion planning’, Int. J. Rob. Res., 2011, 30, (7), pp. 846–894
[44] Kaluder, H., Brezak, M., Petrović, I.: ‘A visibility graph based method for path planning in dynamic environments’, 2011 Proc. 34th Int. Conv. MIPRO 2011, Opatija, Croatia, pp. 717–721
[45] Weiss, A., Danielson, C., Berntorp, K., et al.: ‘Motion planning with invariant set trees’, 2017 IEEE Conf.

Control Technol. Appl. 2017, pp. 1625–1630
[46] Danielson, C., Weiss, A., Berntorp, K., et al.: ‘Path planning using positive invariant sets’, 2016 IEEE 55th Conf. Decis. Control 2016, pp. 5986–5991
[47] Marchese, F.: ‘Time-Invariant Motion Planner in Discretized C-Spacetime for MRS’, (Ed.): ‘Multi-Robot Systems, Trends and Development’, (InTech, 2011), pp. 307–324
[48] Liu, C., Lee, S., Varnhagen, S., et al.: ‘Path planning for autonomous vehicles using model predictive control’, 2017 IEEE Intell. Veh. Symp. 2017, pp. 174–179
[49] Yuan, K., Shu, H., Huang, Y., et al.: ‘Mixed local motion planning and tracking control framework for autonomous vehicles based on model predictive control’, IET Intell. Transp. Syst., 2019, 13, (6), pp. 950–959
[50] Huang, Y., Ding, H., Zhang, Y., et al.: ‘A Motion Planning and Tracking Framework for Autonomous Vehicles Based on Artificial Potential Field Elaborated Resistance Network Approach’, IEEE Trans. Ind. Electron., 2020, 67, (2), pp. 1376–1386
[51] Zhang, X., Sun, J., Qi, X., et al.: ‘Simultaneous modeling of car-following and lane-changing behaviors using deep learning’, Transp. Res. Part C Emerg. Technol., 2019, 104, (May), pp. 287–304
[52] Nguyen, H., Kieu, L.-M., Wen, T., et al.: ‘Deep learning methods in transportation domain: a review’, IET Intell. Transp. Syst., 2018, 12, (9), pp. 998–1004
[53] Vallon, C., Ercan, Z., Carvalho, A., et al.: ‘A machine learning approach for personalized autonomous lane change initiation and control’, 2017 IEEE Intell. Veh. Symp. 2017, pp. 1590–1595
[54] Lenz, D., Diehl, F., Le, M.T., et al.: ‘Deep neural networks for Markovian interactive scene prediction in highway scenarios’, 2017 IEEE Intell. Veh. Symp. 2017, pp. 685–692
[55] Ziebart, B.D., Maas, A., Bagnell, J.A., et al.: ‘Maximum entropy inverse reinforcement learning’, Proc. Natl. Conf. Artif. Intell. 2008,
[56] Herman, M., Fischer, V., Gindele, T., et al.: ‘Inverse reinforcement learning of behavioral models for online-adapting navigation strategies’, Proc. - IEEE Int. Conf. Robot. Autom. 2015,
[57] Bojarski, M., Del Testa, D., Dworakowski, D., et al.: ‘End to End Learning for Self-Driving Cars’, 2016, 48, pp. 1–9
[58] Sharath, M.N., Velaga, N.R., Quddus, M.A.: ‘A dynamic two-dimensional (D2D) weight-based map-matching algorithm’, Transp. Res. Part C Emerg. Technol., 2019, 98, pp. 409–432
[59] Choset, H., Lynch, K.M., Hutchinson, S., et al.: ‘Potential Functions’, (Ed.): ‘Principles of Robot Motion: Theory, Algorithms, and Implementations’, (MIT Press, 2005),
[60] NGSIM: ‘Next generation simulation’, U.S. Dep. Transp., 2007
[61] Thiemann, C., Treiber, M., Kesting, A.: ‘Estimating Acceleration and Lane-Changing Dynamics from Next Generation Simulation Trajectory Data’, Transp. Res. Rec. J. Transp. Res. Board, 2008, 2088, (1), pp. 90–101
[62] Montanino, M., Punzo, V.: ‘Trajectory data reconstruction and simulation-based validation against macroscopic traffic patterns’, Transp. Res. Part B Methodol., 2015, 80, pp. 82–106
[63] Punzo, V., Borzacchiello, M.T., Ciuffo, B.: ‘On the assessment of vehicle trajectory data accuracy and application to the Next Generation SIMulation (NGSIM) program data’, Transp. Res. Part C Emerg. Technol., 2011, 19, (6), pp. 1243–1262
[64] Zheng, L., Jin, P.J., Huang, H., et al.: ‘A vehicle type-dependent visual imaging model for analysing the heterogeneous car-following dynamics’, Transp. B Transp. Dyn., 2016, 4, (1), pp. 68–85
[65] Treiber, M., Hennecke, A., Helbing, D.: ‘Congested traffic states in empirical observations and microscopic simulations’, Phys. Rev. E, 2000, 62, (2), pp. 1805–1824
[66] Kesting, A., Treiber, M., Helbing, D.: ‘General Lane-Changing Model MOBIL for Car-Following Models’, Transp. Res. Rec. J. Transp. Res. Board, 2007, 1999, (1), pp. 86–94
[67] Krajewski, R., Bock, J., Kloeker, L., et al.: ‘The highD Dataset: A Drone Dataset of Naturalistic Vehicle Trajectories on German Highways for Validation of Highly Automated Driving Systems’, 2018 21st Int. Conf. Intell. Transp. Syst. 2018, pp. 2118–2125
[68] Zhang, C.: ‘Path Planning for Robot based on Chaotic Artificial Potential Field Method’, IOP Conf. Ser. Mater. Sci. Eng. 2018, p. 012056
[69] Kala, R.: ‘Potential-Based Planning’, (Ed.): ‘On-Road Intelligent Vehicles: Motion Planning for Intelligent Transportation Systems’, (Elsevier, 2016), pp. 318–356
[70] Cao, P., Xu, Z., Fan, Q., et al.: ‘Analysing driving efficiency of mandatory lane change decision for autonomous vehicles’, IET Intell. Transp. Syst., 2019, 13, (3), pp. 506–514
[71] Deo, N., Rangesh, A., Trivedi, M.M.: ‘How Would Surround Vehicles Move? A Unified Framework for Maneuver Classification and Motion Prediction’, IEEE Trans. Intell. Veh., 2018, 3, (2), pp. 129–140
[72] SAE: ‘Surface Vehicle Recommended Practice: (R) Taxonomy and Definitions for Terms Related to Driving Automation Systems for On-Road Motor Vehicles’, SAE Int., 2018, J3016, pp. 1–35